Hybrid photocathodes for carbon dioxide reduction: interfaces for charge separation and selective catalysis

D. A. Garcia Osorio,[1] Dr G. Neri[1] and Prof   A. J Cowan[1*]

[1] Department of Chemistry and Stephenson Institute for Renewable Energy, University of Liverpool, Liverpool, UK, L69 7ZF. acowan@liverpool.ac.uk

Abstract

Light-driven carbon dioxide reduction at photocathodes was first reported over 40 years ago, however the efficiency and stability of the state-of-the-art lies behind of water splitting photocathodes and photoanodes. Issues have included the low selectivity's towards carbon dioxide reduction (versus hydrogen evolution) and short charge separation lifetimes. "Hybrid" photocathodes, where a light absorbing semiconductor is used with a selective molecular electrocatalyst, are now emerging as a promising way to address these issues. Here we provide a review of hybrid photoelectrodes reported for CO_2 reduction. Focusing on the semiconductor/molecular catalyst interface, we evaluate the operating principles and design features of the materials reported to date and propose new directions for the field.

1. Introduction: Enabling the use of solar energy to meet the world's energy demands is one of the greatest challenges of modern society. However, the intermittent nature of sunlight means that efficient ways to store and transport the captured energy need to be found. Using

solar energy to produce high value chemicals and feedstock is regarded as one such way.[1] In particular, the light-driven conversion of water and CO_2 into carbon based fuels and feedstock is particularly attractive, as the products can be readily introduced into existing chemicals and energy infrastructure.[2–5]

Electrochemical CO_2 reduction, which can be coupled to photovoltaics, has progressed significantly in the last 10 years, and is reviewed extensively elsewhere.[6–9] Although significant challenges remain and concerns persist about the overall system cost, attempts are being made to commercialise CO_2 electrolysis.[10] Photocatalytic CO_2 reduction is a potentially lower cost pathway to solar carbon fuels, but a less mature field. There are many examples of photocatalysts that can carry out CO_2 reduction, or water oxidation, in the presence of sacrificial electron donors or acceptors[11–13], but relatively few that can carry out both half reactions efficiently.[14] Photoelectrochemical (PEC) conversion of CO_2 (figure 1a) represents an alternative approach where the cathode for CO_2 reduction is also a light absorbing material and analyses indicate that PEC CO_2 reduction may offer a balance between cost/complexity of system and efficiency.[15–19] Here we review a particular class of CO_2 reduction photocathodes: hybrid materials composed of a selective molecular electrocatalyst and either a light-absorbing semiconductor electrode or a dye-sensitised electrode. Within the field of hybrid photocathodes, a range of light absorber/catalyst interfaces have now been reported (figure 1 b-e). Following a brief introduction to the principles of photoelectrochemistry and the challenges of achieving selective CO_2 catalysis we discuss each interface type, highlighting the benefits and disadvantages of the different structures used in state-of-the-art materials.
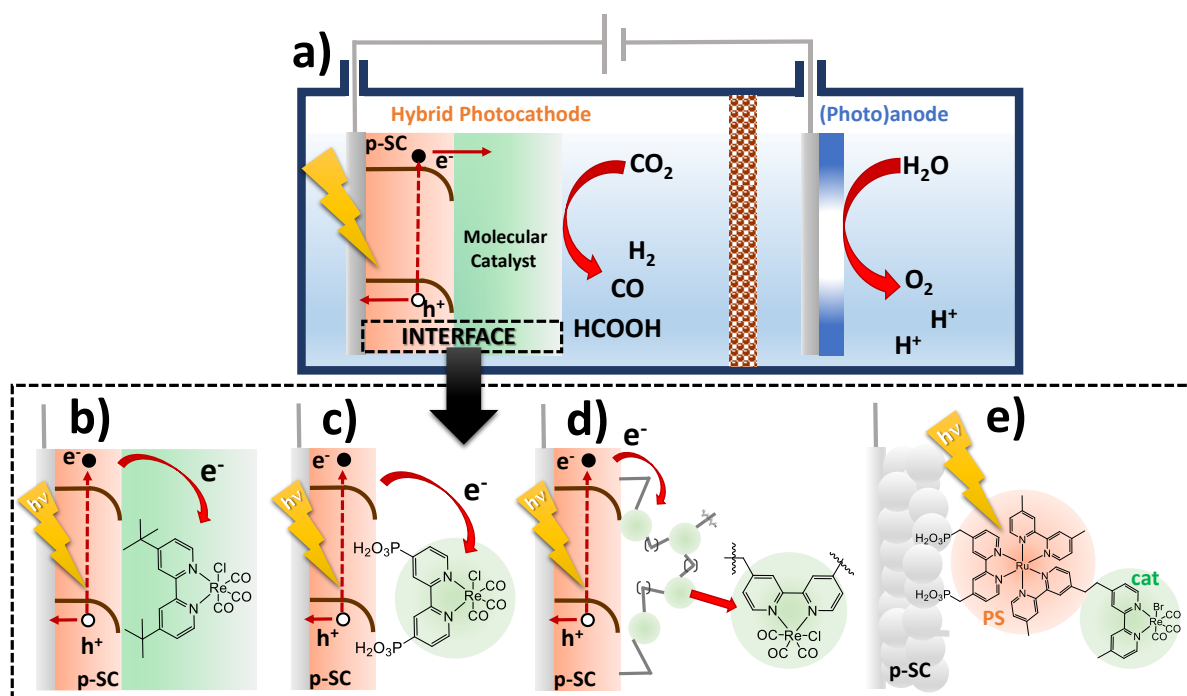
Figure 1. *(a) Schematic illustration of an hybrid p-semiconductor (p-SC) photocathode and (photo) anode in a photoelectrochemical cell for CO_2 reduction.*[17] *Types of interface between the catalyst (green) with the light absorber material (orange) discussed: (b) molecular catalyst in solution,*[20] *(c) covalently bound to the semiconductor,*[21] *(d) electropolymerised,*[22] *(e) and supramolecular catalyst composed by a photosensitiser (PS) and catalyst (cat).*[23]

2. Conventional semiconductor photocathodes: Prior to discussing the design of hybrid photocathodes, it is first necessary to include a very brief summary of the operating principles of a photocathode in the absence of a catalyst. Initially we discuss an ideal semiconductor (one with a low density of surface states) before addressing non-ideal behaviour, which is often observed with many semiconductors of interest for CO_2 reduction. Interested readers are directed to more thorough reviews of the principles of semiconductor photoelectrochemistry that cover the material introduced here in a greater level of detail.[24,25]

2.1 Ideal p-type semiconductor-electrolyte interface: In a p-type semiconductor, the Fermi level (E_F) is located above the valence band edge, figure 2a. When the semiconductor is immersed in an electrolyte with a redox Fermi level (E_{red}) that lies above E_F, the difference between E_F and E_{red} leads to a transfer of charge from solution to the semiconductor, until

3

equilibrium is achieved ($E_F = E_{red}$), figure 2b. The accumulation of electrons in the semiconductor generates a negatively charged region close to the semiconductor liquid junction (SCLJ) and the negative charge in the semiconductor is balanced by a rearrangement of electrolyte ions within the double layer structure. This charge redistribution generates an electric field that varies linearly with distance from the interface in an ideal semiconductor. Hence a parabolic variation in potential across the space charge region occurs and the energy of the electrons and holes is modified giving rise to bending of the valence (E_V) and conduction bands (E_C) on the energy level diagrams, figure 2b.[6,26]
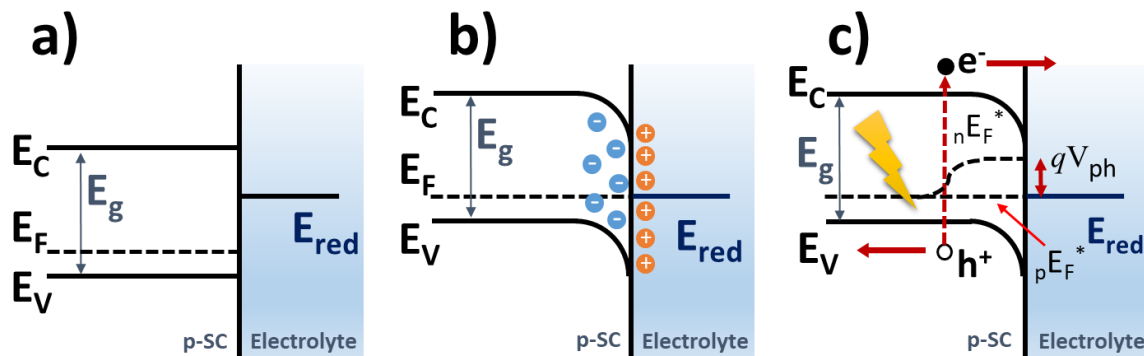
Figure 2. *Band diagrams of a p-type semiconductor (a) before, (b) after the equilibrium with the electrolyte, and (c) under illumination.*[6,26,27] *$_nE_F^*$ and $_pE_F^*$ are the quasi electron and quasi hole Fermi levels, respectively.*

Under illumination with photons of higher energy than the band gap (E_g), a hole-electron pair is created within the semiconductor. When photon absorption occurs within the space charge region the electric field present facilitates charge separation[28] with the migration of electrons towards the semiconductor surface and holes being moved into the bulk of the semiconductor (figure 2c). Additionally, the decreased majority charge carrier (hole) concentration close to the SCLJ lowers recombination rates, further increasing the probability of charge carrier separation. As a result of this charge separation is often assumed to occur with unity efficiency

within space charge region.[24] In contrast, within the bulk of the semiconductor where the hole

concentration is high, recombination rates of photogenerated charges will be significantly

greater. The subsequent low levels of charge separation within the bulk means that only

photoelectrons generated within the distance of the minority carrier diffusion length of the

space charge region are likely to reach the semiconductor surface. Once at the

electrode/electrolyte interface, the ability of the electrons to drive the desired reduction (e.g.

CO_2 reduction) in a net forward manner is given by the electron quasi-Fermi level ($_nE_F*$), a

concept illustrated in figure 2c where $_pE_F*$ is the hole quasi-Fermi level and V_{ph} the available

photovoltage for the overall electrochemical reaction.[26]

As the probability of electron-hole separation is far greater in the space charge region than in

the bulk, it is important to briefly address the factors controlling the width and potential drop

across the space charge region. Nominal widths of the space charge region (W_{sc}) of ~10-100's

nm are often quoted in reports, but equation 1 (where ε_0 is the vacuum permittivity and q the

elementary charge) shows that W_{sc} depends on the doping density (N_d), potential drop across

the space charge region ($\Delta\phi_{sc}$) and the relative permittivity of the semiconductor material (ε).

$$W_{sc} = \left(\frac{2\Delta\phi_{sc}\varepsilon\varepsilon_0}{qN_d}\right)^{1/2} \quad \text{Eq. 1.}$$

Therefore, through tuning of the dopant concentration and modification of the potential drop

across the semiconductor, typically by applying a bias to the electrode, it is possible to vary

W_{sc} and hence the overall efficiency of charge separation under illumination.

2.2 Non-ideality of the semiconductor-electrolyte interface: For an ideal semiconductor-

electrolyte interface it is possible to use the Gärtner equation to calculate the incident photon

to current efficiency for a photocathode and its dependence on applied potential with

knowledge only of W_{sc}, the electron diffusion length and the absorption coefficient for the incoming photons.[29] In reality large deviations from such ideal behaviour are often observed. Amongst the assumptions of the Gärtner model is that electron transfer across the interface is fast, preventing build-up of charge at the SCLJ. As will be discussed in more detail in section 3.1 the rate of electron transfer during CO_2 reduction is likely to be slow in the absence of a catalyst, with the accompanying charge accumulation leading to a change in band bending and increased recombination losses at the interface.

A further complication is that the majority of semiconductors surface states arising from the termination of the lattice can cause non-ideal behaviour. Materials with redox active surface states, *i.e.* those able to undergo electron transfer to/from the bulk semiconductor or to/from species in solution will change the charge distribution at the interface. The occupancy of the states will depend upon E_F, with states filled at values above the energy of the states (E_{SS}) and emptied as E_F is lowered. The changing occupancy of these surface states changes the surface charge of the semiconductor and hence the potential drop across the Helmholtz layer of the electrolyte. As a result, when E_F is at ~E_{SS}, changes in potential primarily occur across the Helmholtz layer and the change in band bending with applied potential is significantly lower than ideal behaviour would predict. Until the surface states are either completely populated or depopulated with electrons, the Fermi level effectively becomes pinned and largely insensitive to applied voltage.[24] In cases where the density of surface states is high enough the potential across the space charge region, and hence the band bending within the semiconductor, is essentially fixed by these surface states and becomes independent of the E_{red} of species in solution, figure 3. It has been shown in photoelectrochemical studies with many common photocathodes including *p*-GaAs, *p*-Si that Fermi level pinning occurs. Although this limits the achievable photovoltage, it does enable photoelectron transfer to a wider range of redox couples in solution including those that may be at a more negative potential than the conduction

band edge in the absence of the redox couple.[30] Surface states can also play an important role in the trapping of photogenerated charges. Trap states lying in energy between the conduction and valence band edges, modify the driving force for charge transfer across the semiconductor/electrolyte (or catalyst) interface and they can also act as recombination centres.[6]
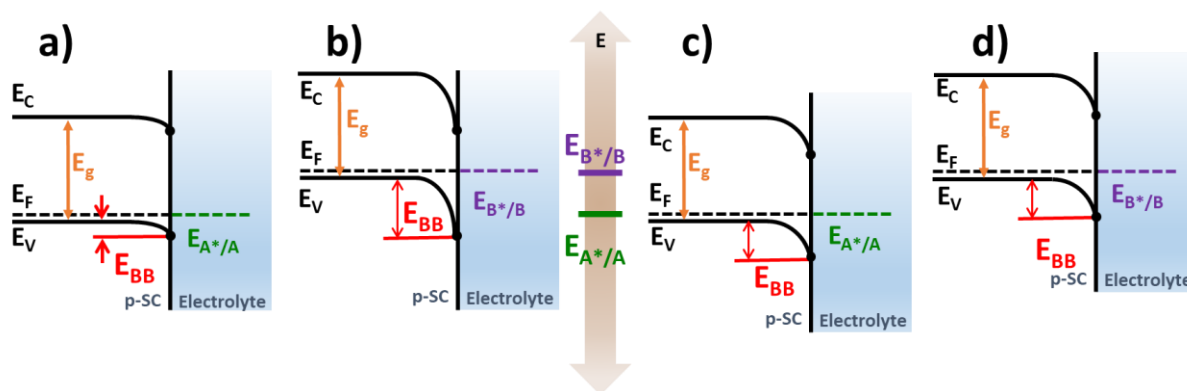
Figure 3. *Interface energetics of a p-SC: (a, b) Band Bending (E_{BB}) dependent on the E_{red}: $E_{A*/A}$, $E_{B*/B}$, and (c, d) Fermi Level Pinning, where E_{BB} is independent of E_{red}. Adapted for a p-type semiconductor from [30].*

Finally, many state-of-the-art CO_2 reduction photocathodes use nanostructured semiconductors as a light absorber. In systems where the particle dimensions approach the Debye length it is not possible to generate a significant level of band bending. In the absence of band-bending new models for charge separation and transport through the electrode need to be considered. The effect of particle dimension on achievable potential drop has been modelled for several different film morphologies including nanoparticle (sphere) and nanorods allowing for prediction of behaviour if the dopant density is known.[31,32] However application of such models to practical systems is complex with the achievable field being dependent not just on the primary particle size but also on the degree of ordering of the primary particles.[25]

It is therefore clear that the result of non-ideal behaviour brought about through nanostructuring and the presence of surface states, including those induced by the formation of the

semiconductor/catalyst interface, can be hard to predict. This makes measurements to determine the mechanisms and kinetics of key processes including charge separation, transport and transfer vital in enabling rational design of hybrid photoelectrodes.

3. PEC CO$_2$ reduction – the need for catalytic sites: Charge transfer at the semiconductor/electrolyte interface to CO$_2$ (or surface CO$_2$ intermediates) is in kinetic competition with competitive charge transfer reactions (e.g. direct to H$^+$ and/or H$_2$O in the hydrogen evolution reaction). Even if hydrogen evolution is minimised, slow kinetics for electron transfer to CO$_2$ are highly undesirable, leading to an accumulation of charge at the interface and a subsequent increase in recombination and an increased probability of trapping of charges in deep-lying states (see section 2.2). Therefore the low availability of CO$_2$, due to its low solubility in aqueous electrolytes (~33 mM),[33] and the thermodynamic stability of CO$_2$ to reduction[34] present a great challenge to achieving efficient PEC CO$_2$ conversion.[35–38] The standard potential for the one electron reduction of CO$_2$ (CO$_2$/CO$_2^{\bullet-}$) is -1.9 V$_{RHE}$.[33] In contrast a range of multi-electron, multi-proton reductions of CO$_2$ are achieved at significantly more positive potentials. The various C$_1$ products that can be obtained from the reduction of CO$_2$ in aqueous solutions are shown in the Latimer-Frost diagram in figure 4.[39] An effective way to enabling the multi-electron, proton, reduction of CO$_2$ and to avoid the formation of CO$_2^{\bullet-}$ is therefore to first transfer the photoelectron to a known CO$_2$ reduction electrocatalyst (figures 1 b-d), as it avoids the need to accumulate charge within the space charge layer. A further advantage is that by judicious choice of electrocatalyst it should be possible to target specific CO$_2$ reduction products and avoid competitive hydrogen evolution.
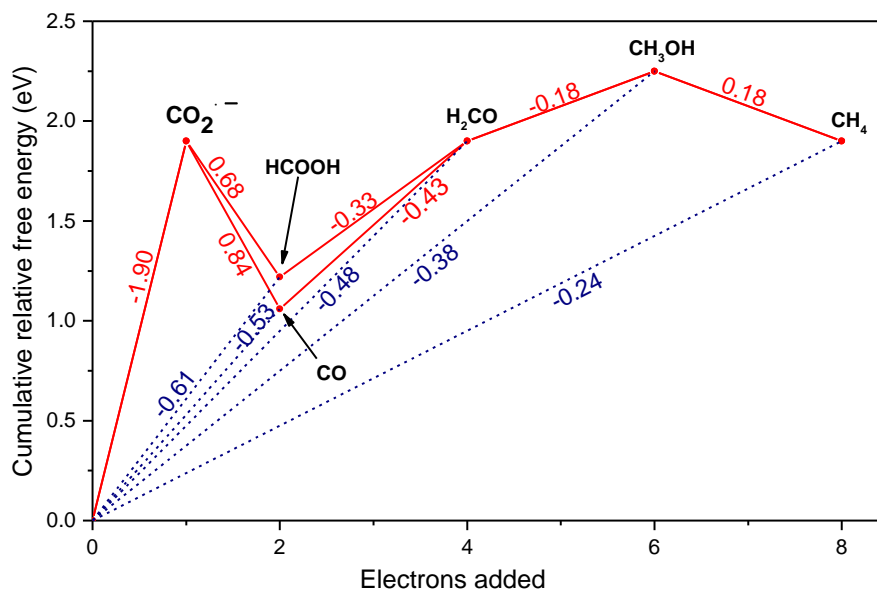
Figure 4. *Latimer-Frost diagram for the possible reduction reactions of CO_2 in water at pH 7 with showing the relative stability for each species (red, eV). Values taken from ref. [39] and references therein. The blue lines show the equilibrium potential for the electrochemical reaction to achieve the indicated products (vs NHE).*

A range of metals have been shown to be effective as electrocatalysts for CO_2 reduction and examples of semiconductor photoelectrodes decorated with metal nanoparticles such as Au, Ag, Ru, In, and Pb are known and these are reviewed elsewhere.[40–43] Here we focus on the use of molecular electrocatalysts (figure 5), typically transition metal complexes with semiconductor absorbers (figure 1b-d). The ability to accumulate multiple charge equivalents,[44–48] and the capability to achieve extremely high turnover frequencies (~10^6 s^{-1}) and selectivities make them an attractive target for use in PEC devices.[49,50] Importantly, the synthetic tunability of molecular catalysts also offers control over the electrode/catalyst interface making it feasible to develop structures that facilitate fast electron transfer from the semiconductor to the catalyst to prevent charge accumulation within the space charge layer to lower recombination losses.

3.1 Molecular electrocatalysts for PEC CO₂ reduction: As research into both molecular electrocatalysts for CO$_2$ reduction[48,51–57] and semiconductor materials for solar fuels production has expanded rapidly in recent years,[11,12] albeit largely independently, there is now a large number of potential combination of catalysts and absorbers. This review does not aim to survey all possible combinations, or even report all of those that have been used to date, but before we go on to cover the different exemplifying types of semiconductor/molecular catalyst interface identified in figure 1, it is important to discuss why and how particular material combinations are often chosen.
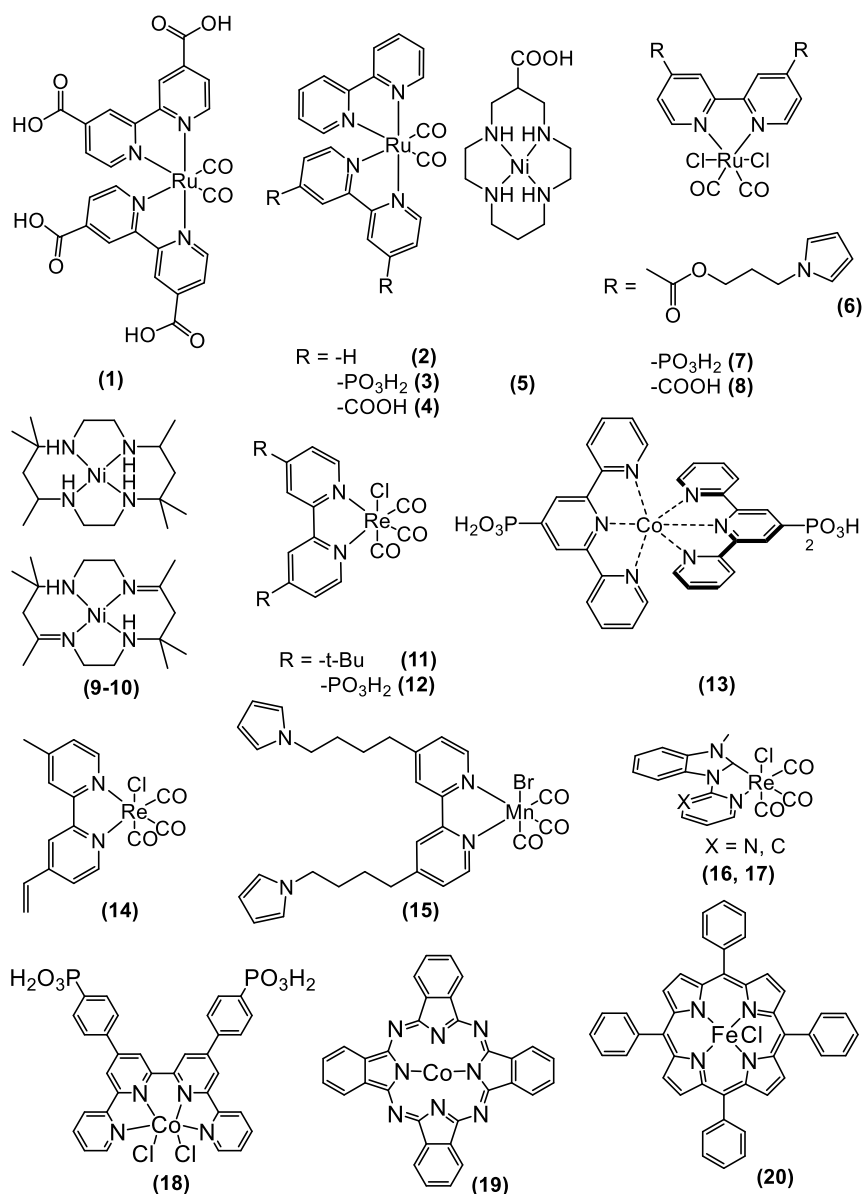
Figure 5. Structures/classes of molecular electrocatalysts that have been coupled to semiconductor photoabsorbers for PEC CO_2 reduction or related catalysts that are discussed in this review. Supramolecular complexes for use in dye sensitized systems are discussed separately below (section 4.4)

For a hybrid electrode to operate effectively a negative change in Gibbs free energy for electron transfer (ΔG_{ET}) from the semiconductor to the molecular catalyst is necessary. This has led to a focus within the literature on hybrid photoelectrodes based on semiconductors with particularly negative conduction band potentials e.g., InP:Zn (-0.915 V_{RHE}),[58] GaP (-1.765 V_{RHE}),[58,59] N-Ta$_2$O$_5$ (-1.165 V_{RHE}),[59] Cu$_2$ZnSnS$_4$ (-0.865 V_{RHE}),[60] Cu$_2$O (-1.2 V_{RHE}).[61]

Most of these are expected to be able to undergo electron transfer to the commonly used classes of molecular electrocatalyst shown in figure 5, based upon the onset potential for CO_2 catalysis with the electrocatalyst either in solution or when immobilised onto an electroactive support (e.g. $[Ru(bpy-R)_2(CO)_2]^{2+}$ (**1-4**) ~ -0.7 to -0.9 V_{NHE}[62], $[Ni(cyclam-R)]^{2+}$ (**5, 9**) ~ -0.9 V_{NHE}[63,64], $[Mn(bpy-R)(CO)_3X]$ (**15**) ~ -0.9 V_{NHE},[65,66] $[Re(bpy-R)(CO)_3X]$ (**11, 12, 14**) ~ -0.9 to -1.2 (typically),[21,67] V_{NHE}, $[Co(tpy-R)_2]^{2+}$ (**13**) ~ -0.8 V_{NHE}[68]).

Comparison of published values of the conduction band edge and the onset of catalysis for the electrocatalyst (E_{cat}) can act as a useful starting point to identify the feasibility of semiconductor-catalyst electron transfer, but this approach overlooks both the possible role of electrode-catalyst interactions on E_{red} (and more importantly E_{cat}) and the presence of semiconductor surface states (see section 2.2). Mechanistic studies show that the surface states can have negative effects preventing charge transfer. For example, transient absorption measurements of N-Ta_2O_5 photoelectrodes with $[Ru(dcbpy)_2(CO)_2]^{2+}$ (**1**) have shown that the presence of deep-lying trap states prevents a fraction of photogenerated electrons from transferring to the catalyst. This is despite the conduction band being ~0.4 V negative of the onset potential of catalysis of (**1**) in solution.[69] Conversely the very high density of surface states and resultant Fermi level pinning of p-Si has facilitated charge transfer in some studies. Some of the earliest reported hybrid photocathodes[30,34,45] achieved photoelectron transfer from p-Si to molecular catalysts despite the conduction band edge being negative of the onset potential for catalysis based off measurements of the isolated components.[30,34,45] For example PEC cells consisting of p-Si and Ni and Co macrocles (**9-10**) were highly selective for CO_2 reduction to CO, indicating successful electron transfer to the catalyst despite the mismatch in E_C and E_{cat}.[70,71] CO_2 reduction has since been reported at p-Si with a range of molecular catalysts including complexes of Re[20] (**11**), Co[72] (**13**) and Mn[73] (**15**), with similar photovoltages being achieved in all cases indicating the occurrence of Fermi level pinning.

3.2. Control of the driving force of electron transfer: As electron-hole recombination within the absorber material is in kinetic competition with electron transfer to the catalyst,[74] it is important to optimise the rate of electron transfer to (and minimise the rate of back electron transfer from) the catalyst. In systems where Fermi-level pinning of the semiconductor is not occurring, control of the driving force for electron transfer can be achieved through synthetic modification of the catalyst to change its reduction/catalytic onset potential. Motohiro *et al.*[75] studied a series of Ru polypiridyl molecular catalysts modified with differing types of binding groups (**2-4**) with an N-Ta_2O_5 absorber for the reduction of CO_2 to HCOOH and CO. In these works, a correlation between the catalyst reduction potential and the overall activity of the hybrid PEC system was observed with the catalysts with the most positive onset potentials for giving rise to the highest turnover numbers (TON's). For example, catalysts with the phosphonic acid binding group (**3**) were found to be catalytically active in solution at potentials +0.1 V positive of those with carboxylic acid groups (**4**), with the increased driving force for charge transfer being proposed for the increase in TONs from 24 (HCOOH) and 17 (CO) with **4**, to 118 (HCOOH) and 76 (CO) with **3**. The works of Motohiro and Morikawa demonstrate that synthetic modification of the catalyst can be used to tune the driving force for electron transfer. Similarly, through modification of the semiconductor absorber, the efficiency of electron transfer can also be changed. Some of us have previously used transient absorption spectroscopy to directly measure the rate of electron transfer from both TiO_2 and $Ti_{1-x}Zr_xO_2$ absorbers to a modified $Ni(cyclam)^{2+}$ (cyclam = 1,4,8,11-tetraazacyclotetradecane) catalyst (**5**), and shown that the negative shift in E_C for $Ti_{1-x}Zr_xO_2$ of *ca.* 150 mV led to a ~50% increase in the rate of electron transfer and enhanced charge separation lifetimes.[76] However, it is important to reiterate that the factors controlling charge transfer are numerous and often interdependent making it hard to predict behaviour. Multiple reports that showed no correlation between PEC activity and predicted ΔG_{ET} based off isolated measurements of the catalyst and

semiconductor. For example the behaviour of Cr_2O_3/N,Zn-Fe_2O_3/TiO_2 hybrid photoelectrodes was dominated by the binding mode and its strength between the molecular catalyst and the TiO_2 layer,[77] similarly studies on Ru catalysts (**6-8**) with N-Ta_2O_5, GaP, and InP indicated that PEC activity was controlled by the nature (e.g. geometry of components and the electronic structure) of the interface formed.[59]

4. Interfacing the catalyst and light absorber: It is therefore clear that whilst identification of catalyst/absorber combinations with a predicted driving force to enable efficient charge transfer across the semiconductor/catalyst interface is an appropriate starting point for designing new hybrid photocathodes, there is a need to move beyond analysis of materials based on the isolated electrochemical properties of the individual components. Factors such as catalyst immobilisation method, orientation at the surface, presence of charge transfer pathways, and the role of immobilisation on the catalytic mechanism can instead dominate the overall activity of photoelectrodes. In the following section, we categorise and examine examples of catalyst/absorber interfaces reported in literature.

4.1 Early studies of hybrid electrodes - catalysts in solution: Within 5 years of the first reports of PEC CO_2 reduction, studies using molecular catalysts in solution began to appear (figure 1b).[42,70,71] A common feature of early works was an improved selectivity towards a specific CO_2 reduction product, for example using a CdTe absorber with a cobalt phthalocyanine complex, Bockris achieved ~100% Faradaic efficiency (FE) for CO production.[42] A particular focus of early studies was the use of Ni(cyclam)$^{2+}$ and derivatives (**9-10**), catalysts known to be highly selective for CO_2 reduction in water to CO,[78] with a range of p-type semiconductor such as p-Si[70,71] p-GaP, p-GaAs.[79] Experiments with p-Si were initially carried out in acetonitrile-water mixes,[70,71] but soon studies with p-GaAs in water[79,80]

were also made. In all cases addition of **9-10** led to a significant change in product distribution confirming their catalytic role, with CO again becoming the dominant product formed, while in the absence of the catalysts H_2 was produced. Notably the total charge passed also increased in the presence of the Ni catalysts, and photocurrent onset potentials shifted positive. The ease of use of a photoelectrode and catalyst in solution has meant that approach is still relatively widespread with recent examples including the use of *p*-Si with both Re(bpy)(CO)₃Cl derivatives [20] and iron porphyrin complexes (**20**) [81] (both for CO production) and *p*-GaP with pyridine for methanol production in water.[82]

The approach of using the catalyst in solution does have several disadvantages: (1) the high concentration of catalyst in solution can cause parasitic light absorption, (2) large portions of the catalyst are not in contact with the semiconductor surface at any one-time decreasing the probability of charge transfer,[83,84] (3) the nature/orientation of the catalyst-electrode interaction is hard to control and highly dependent on the electrolyte[54], light intensity and the applied potential[70,85] and some molecular catalyst maybe be decomposed during long illumination periods.[57] For example, in a recent study of Re-N-heterocyclic carbene complexes (**16** and **17**) with a *p*-Si photocathode, addition of 5% water to an acetonitrile electrolyte was found to be sufficient to prevent one of the two catalysts studied adsorbing onto the photocathode.[86] Finally, (4) under conditions where the photoelectron flux is relatively low, it is also feasible that diffusion of partially reduced species away from the electrode surface may occur prior to completion of the catalytic cycle.

4.2 Polymerised catalysts – generating charge transport pathways and imparting stability: Immobilisation of molecular catalysts (Figure 1c-e) onto the semiconductor surface aids separation of liquid products from the catalyst materials, decreases the amounts of catalyst needed, and in some studies it has also been shown to improve the rate of interfacial electron transfer from the semiconductor to the catalyst.[76,84,87] One of the most effective methods to

15

adhere catalysts to semiconductors surfaces is through electropolymerisation (figure 1d).[59,60,88] Over 30 years ago [Re(vinyl-bpy)(CO)$_3$Cl] (**14**), a derivative of a widely studied class of Re carbonyl electrocatalysts, was reductively (photoelectrochemically) polymerised onto both p-Si and p-WSe$_2$ photocathodes in CH$_3$CN based electrolytes.[89] In this study, a photovoltage of ~0.6 V (with p-Si) was achieved leading to CO$_2$ catalysis occurring at more positive applied potentials when compared to the complex deposited onto Pt. More recently, the polymerisation of catalysts onto light absorbing semiconductors has also been used to achieve photoelectrochemical reduction of CO$_2$ with a related Mn bipyridine complex (**15**).[73] In this study p-type hydrogen-terminated Si nanowires were used as the light absorber, and although product analysis was not carried out for the hybrid photocathode, the cyclic voltammograms under CO$_2$ and light illumination (in a MeCN solution with 5% water) showed a significant increase of the current density compared to the Ar and dark curves.

Polymerisation does offer several advantages over the other methods of catalyst immobilisation described below. Morikawa and coworkers[58] demonstrated that electron transfer pathways between the semiconductor surface and the catalyst (and in between catalytic centres) can be formed in a study using a Ru catalyst that generates a conductive polypyrrole polymer (**6**). Furthermore, polymerisation offers the possibility to generate thick polymer coatings containing a high concentration of catalytic sites on the semiconductor. For example a 110 nm thick layer based on a Ru(**6**) precursor was deposited on a Cr$_2$O$_3$/N,Zn-Fe$_2$O$_3$/TiO$_2$/**6** photoelctrode.[77] A further benefit of the thick polymer catalyst layer in this study was that it provided a protective layer over the absorber with the polymerised catalyst photoelectrode achieving a stable photocurrent (150 µA cm^{-2}) over a 13 hour period to produce HCOOH, CO with a high Faradic efficiency (63% and 30% respectively). In contrast rapid (minutes) degradation of the Cr$_2$O$_3$/N,Zn-Fe$_2$O$_3$/TiO$_2$ structure occurred with similar Ru complexes when -PO$_3$H$_2$ and -COOH anchoring groups (**7-8**) were used.[77] In addition to these works, a number

16

of other photocathodes have now been studied with polymerised Ru catalysts for CO_2 reduction with highlights including the use of **6** electropolymerised on a *p*-type InP:Zn wafer[58] which was able to produce formate in water with a FE of 62.3% when bulk electrolysis was carried out at -0.6 V_{NHE} under visible illumination.

Although control of the catalyst orientation at the electrode surface is not usually possible through polymerisation, an interesting approach to control and develop a better defined interface for charge transfer is the use of a catalyst with functionality that enables covalent binding to the semiconductor surface alongside a polymerisable catalyst. In studies using Cu_2ZnSnS_4 (CZTS)[60] and InP[59] photoelectrodes mixtures of **6** and **7** were found to lead to higher rates of CO_2 reduction to formate than when either catalyst was used in isolation. It was proposed that the phosphonate groups of **7** enabled binding to the surface of the sulphide and phosphide semiconductors and that **7** acts as an electron transfer facilitator to the conductive polymer network generated by **6**.

In some cases, it has been proposed that the polymer support is also either to act as the catalyst itself or help facilitate the catalytic reduction of CO_2. For example polypyrrole based photoelectrodes exhibited a FE of 62% for CH_3COOH production,[90] while polyaniline based photoelectrodes achieved a FE of 78% for the same reaction.[91]

Recently, a *p*-Si/TiO_2/polymer-Co(**13**) photoelectrode for CO_2 reduction to CO was developed by Reisner and co-workers[92] with the polymer containing 3 different sets of functionalities: (i) phosphonic acid groups to enable binding to the *p*-Si/TiO_2 absorber, (ii) terpyridine ligands for coordinating Co^{2+} to generate a derivative of complex **13** metal center and (iii) hydrophobic functional groups to modify the second coordination sphere of the molecular catalyst and improve CO_2 diffusion across the polymer.

4.3 Covalent immobilisation of catalysts: Covalently binding the catalyst onto the light absorbers surface, or onto a protective coating, provides a way to generate well-defined photoelectrode-catalyst interfaces. In principle such control enables the tuning of the efficiency of charge transfer through modification of the chemical functionality of the binding group and by controlling the catalyst binding angle. A range of possible binding groups to oxide, sulphide and selenide based semiconductors are known,[93–95] with the majority of the literature for oxide surfaces coming from the dye-sensitised solar cell (DSSC) community.[96] These works can be used as inspiration for the design of ligands for catalyst immobilisation with one important caveat: most DSSCs work in organic solvents, and the stability of the anchoring groups will change in a CO_2 reduction PEC cell that uses either an aqueous environment or an organic solvent containing an acid source.[97]

In general, a good anchoring group should react to form a functionality that is resistant to detachment from the surface, promote charge transfer, be able to withstand the reducing environment during catalysis and be stable to long-term light exposure. These requirements apply to both the catalyst in a PEC or catalyst and dye in a Dye Sensitised Photoelectrochemical Cell (DSPEC, see section 4.4). Historically carboxylates and phosphonates are the most widely studied and employed anchoring groups as they bind well to oxide semiconductors (figure 6).[96] Although in aqueous solvents phosphonic acid binding groups offer greater stability than carboxylic acids, the rate of charge transfer to/from the surface bound molecules has been shown to be significantly slower with phosphonic acid groups.[98] In studies of DSSC, this change in rate of charge transfer has been ascribed to the nature of the sp^2 hybridised –COOH group which enables electron delocalisation, in contrast the sp^3 phosphonic group effectively acting as an insulator between the semiconductor and bound molecule.[96] Theoretical studies of the rate of electron transfer from N-Ta_2O_5 to Ru(bpy-R_2)($CO)_2Cl_2$ (R = PO_3H_2 (**7**) and CO_2H

(**8**) have also assigned the faster electron transfer to **8** to be due to increased nonadiabatic coupling between the donor and acceptor sites.[99]

A large number of molecular electrocatalysts have now been modified with phosphonic and carboxylic acids for immobilisation, and used in photocatalytic CO_2 reduction, with examples including derivatives of $Ni(cyclam)^{2+}$, $Ru(bpy)(CO)_2Cl_2$. $Re(bpy)(CO)_3Cl$ and Co(II) bis(terpyridine)[56,62,68,100] with covalent immobilisation being shown by transient absorption spectroscopy to facilitate electron transfer to the catalysts, when compared to the same catalyst in solution.[100,101] However relatively few examples of covalently immobilised CO_2 reduction catalysts on light absorbing photoelectrodes are known.[21,68,75,77,102] An important breakthrough was a study on $Re(bpy-PO_3H_2)(CO)_3Cl$ (**12**) bound to a mesoporous TiO_2 layer coated on Cu_2O/AZO/ALD-TiO_2 (ALD = atomic layer deposition, AZO = aluminium-doped zinc oxide).[21] In previous experiments[83] where an unbound Re catalyst (**11**) was used with a Cu_2O absorber, electrostatic repulsion between the reduced catalyst intermediates and the polarised semiconductor photoelectrode was proposed to prevent multiple charge transfer and subsequent CO_2 reduction. Immobilisation of **12** onto the light absorber overcomes the repulsion of the catalyst from the electrode surface.[21] Initial studies where the catalyst was bound directly onto the smooth ALD TiO_2 layer (used with AZO to both protect, and form a charge separation junction with the Cu_2O[61,103]) resulted in very low catalyst loadings. Under 1 sun the catalyst on ALD TiO_2 was unable to turnover at a sufficiently high rate to keep up with the photogenerated electron flux from the Cu_2O. Once a high surface area mesoporous TiO_2 layer was added catalyst loadings of ~85 nmol cm^{-2} (geometric) were achieved and a large increase in photocurrent occurred. Although this result was an important step for the field, activity decreased within 2 hours under illumination, proposed to be due a combination of catalyst desorption and structural change of the bipyridine ligand of the bound catalyst. As the authors noted immobilisation does bring advantages, facilitating the multi-electron transfers to

the catalyst required for CO_2 reduction, but it does also have a downside. If the catalyst becomes inactive it may remain fixed on to the electrode surface, blocking the regeneration.[21,68] It is therefore important that molecular catalysts for use in hybrid PEC CO_2 reduction are robust under operating conditions, but the stability of the light harvesting material also plays a key role in the performance. Recently, Robert and coworkers[102] developed a hybrid photocathode using a photovoltaic solar cell based on CIGS/CdS/AZO/ZnO and a Co quarpyridine modified with phosphonic groups (Co-qPyH, **18**) anchored to a compact layer of TiO_2. The molecular catalyst loading was 3 ± 1 nmol cm^{-2} and after 2 hours of electrolysis at -0.06 V vs NHE the photocurrent decresed from -3 to ∼-0.5 mA cm^{-2}, however a remarkable selectivity of 97% towards CO was attained and only 3% for H_2 despite the fact that the hybrid photocathode operated only in aqueos electrolyte (0.1 M $KHCO_3$ saturated with CO_2, pH 6.8). In this case, the authors also pointed out the decrease in the photocurrent could be associated either to the desorption of the molecular catalyst or to the degradation of the photovotaic solar cell if the electolyte reached the AZO layer, concluding that an increase of TiO_2 surface area could add extra protection to the solar cell and allow higher loadings of Co-qPyH to improve the performace.

In section 4.2 we discussed the application of a cobalt bis(terpyridine) catalyst[92] in a polymer matrix on p-Si/TiO_2 and a similar system in the absence of the polymer where a phosphonated cobalt bis(terpyridine) (**13**) was bound directly to the p-Si/TiO_2 absorber has also been reported.[68] In addition to being built using entirely earth abundant elements and being able to work in water, this work was notable for the reasonable level of stability achieved, with > 8 hrs of activity reported without significance loss in activity. Following in-situ spectroelectrochemical studies the stability (and improved onset potential) of **13** was proposed to be due to a change in CO_2 reduction mechanism of the catalyst upon immobilisation, figure 7. In contrast to solution where cobalt bis(terpyridine) catalysts undergo loss of one terpyridine

20

ligand prior to CO_2 binding, which can be irreversible if the ligand diffuses away, the catalyst immobilised onto the TiO_2 scaffold was thought to retain its bis(terpyridine) ligation with only a single Co-N site being detached to enable CO_2 binding, figure 7.
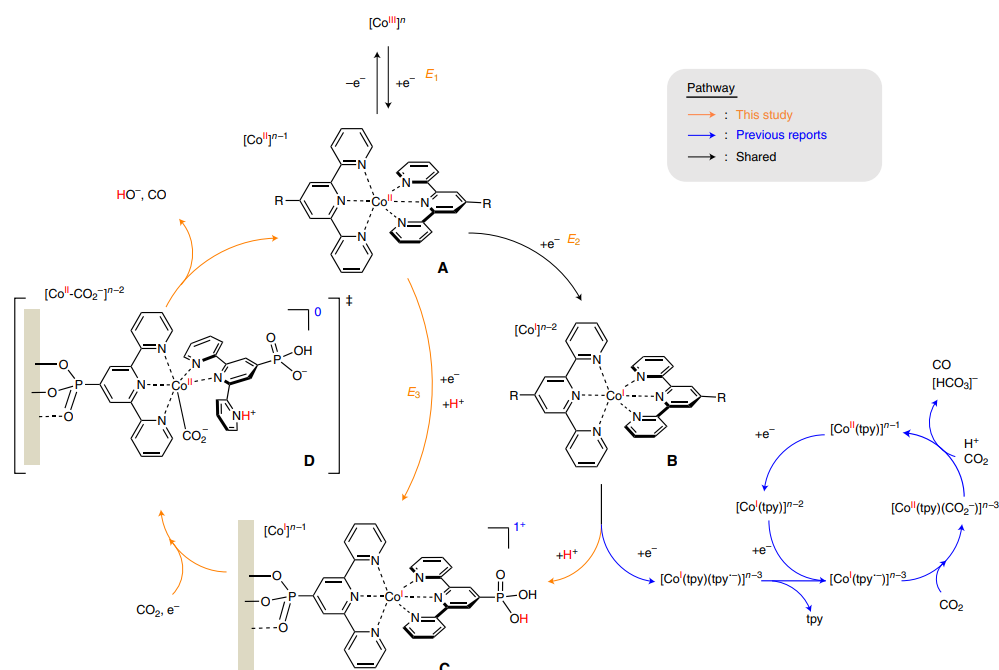
Figure 6. *Proposed mechanism for CO_2 reduction by **13** bound to meso-TiO_2 (orange pathway), in contrast to catalyst in solution (blue pathway). Reproduced with permission from* [68]

Catalyst desorption has been reported to occur even when phosphonic acid binding groups are used, and to reach a level of stability where devices are of practical use orders of magnitude increases in stability are required.[21,102] Recently, within the PEC water splitting community, hydroxamates and silatrane groups have been explored as alternative anchor groups. Carboxylates and phosphonates hydrolise at moderate pH values (pH >4 for carboxylates, pH > 7 for phosphonates). Hydroxamates and silatranes have been found to be stable across a much greater pH range (2-10 and 2-11, respectively). Silatranes have been reported to have similar injection rates than phosphonate when the anchors were used to bind a porphyrin dye to TiO_2 in a DSSC cell. Hydroxamates offer a particularly exciting opportunity, having been shown to

have faster charge injection rates compared to even carboxylic acids when equivalent dye centres and semiconductors are used.[104] Although we do not believe hydroxamates have been used in a PEC CO_2 device yet, they have been applied to PEC hydrogen evolution. Gong and co-workers modified a Cobaloxime with carboxylic, phosphonic and hydroxamates anchoring groups and studied the effect of the anchoring group on the surface of p-Si/TiO$_2$.[105] This study demonstrated that hydroxamates moieties displayed superior capabilities in aqueous electrolytes, generating higher photocurrents, achieving faster electron transfer and better stabilities when compared with the hybrid photocathodes constructed with carboxylic and phosphonic groups.

4.4 – Dye and supramolecular constructs: Turnover frequencies as high as 10^6 s^{-1} for CO_2 reduction to CO have been reported for some Fe porphyrin electrocatalysts under idealised conditions,[50] however the kinetics of the CO_2 reduction reactions of many molecular catalysts under operating conditions can be much slower (e.g. Re(bpy)(CO)$_3$Cl k_{cat} ~150 s^{-1}, CH_3CN[106]). Therefore potential kinetic competition between back electron transfer from the catalyst to the semiconductor can become limiting.[68,69,84,107] In part, this can be overcome through the use of a greater number of catalysts immobilised on high-surface area supports, in the manner described above for Cu$_2$O/AZO/ALD-TiO$_2$/m-TiO$_2$/**12** [83] and Si/m-TiO$_2$/**13** electrodes.[68] Alternatively the lifetime of the charge separated state can be increased through modulation of the internal electric field of the semiconductor,[76] the use of multi-layer solid-state structures[102,108] or by the design of supramolecular constructs for energetic and longer range (spatial) charge separation.[109]

In particular an exciting approach to building photocathodes for CO_2 reduction has emerged, based on the field of dye-sensitised solar cells, which makes use of supramolecular structures to generate long-range charge separated states (figure 1e).[110–113] In this kind of hybrid photocathodes, rather than using a narrow band-gap semiconductor as the light absorber, a wide

band-gap material is used as a hole transporting substrate, and a molecular photosensitiser is used as the light harvesting material.[87,114] The cascade of events that leads to CO_2 reduction is: 1) the photosensitiser or dye (PS) absorbs the light, 2) the wide band-gap semiconductor, usually NiO, can efficiently extract holes from the excited photosensitiser 3) electron transfer from the reduced photosensitiser to the catalyst (cat) occurs and finally 4) CO_2 reduction takes place at the molecular catalyst, as indicated in figure 7.[114] The resultant charge separated state is with the electron residing on the catalyst and the hole on the semiconductor, with the neutral dye molecule between them. Such dye-sensitised photoelectrosynthesis cells (DSPEC) are closely related to dye sensitized photocatalysts for CO_2 reduction and these have been recently reviewed in detail and will not be further discussed here where we only consider DSPEC.[56]
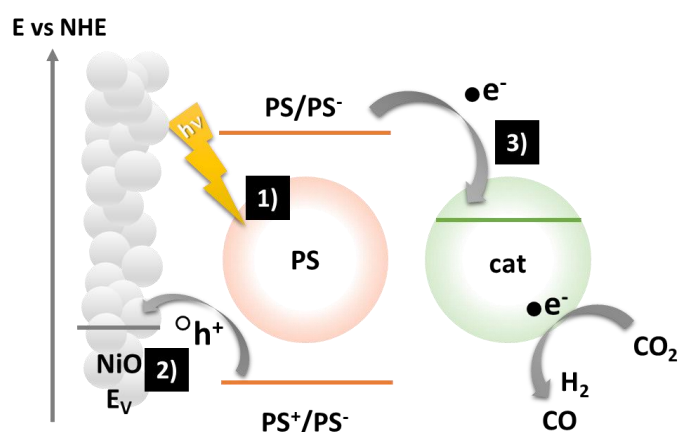
Figure 7 Working principle of a DSPEC (1) the photosensitiser or dye (PS) absorbs the light, (2) the wide band-gap semiconductor extract holes from the excited photosensitiser (3) electron transfer from the reduced photosensitiser to the catalyst (cat) occurs and (4) CO_2 reduction takes place at the molecular catalyst, figure adapted from reference [87].

The first DSPEC for CO_2 reduction that we are aware of was reported in 2014 by Kou et al.,[110] which made use of a NiO hole transport layer coupled to a Zn-Porphyrin and Re-bipyridyl absorber–catalyst supramolecular assembly anchored using carboxylic acid groups. The device was able to convert CO_2 to CO under 420 nm light in a DMF electrolyte. Quenching of the supramolecular assembly emission occurred with a lifetime of ~29 ps suggesting ultrafast

electron transfer from NiO to the dye. Interestingly, the addition of further carboxylic acid functionalised Zn-Porphyrin groups to the NiO electrode surface led to a >5-fold enhancement in activity, assigned to the improved light harvesting and electron transport capabilities of the device. Ishitani et al. [111] examined activity of a Ru-Re supramolecular assembly covalently bound to NiO *via* phosphonate groups. The photoelectrode produced exclusively CO in a DMF/TEOA solution. Significantly the same group reported the ability of this DSPEC to carry out CO_2 reduction in water when coupled to a water oxidation CoO_x/TaON photoanode, with selectivity retained for CO production.[112] The DSPEC produced 361 nmol of CO and 36 nmol of H_2 at a potential of -0.7 $V_{Ag/AgCl}$ under illumination. Studies using the same Ru-Re supramolecular assembly on a $CuGaO_2$ electrode later achieved bias free CO_2 reduction when used in conjunction with a CoO_x/TaON photoanode.[113]

In an attempt to increase both the stability of the NiO-assembly binding and the loading of the dye/catalyst assembly Ishitani et al.[23] polymerised vinyl modified Ru-Re dyads (figure 8) which also contained a phosphonate group (in a strategy similar to described in section 4.2).[59,77] The polymerised dyad was present at loadings of > 30 nmol cm^{-2} and only a small fraction of the complex was lost during ~5 hrs of use of the photoelectrode. Overall an IPCE of 0.93% (480 nm, -0.5 $V_{Ag/AgCl}$) and high Faradaic efficiency for CO production was achieved. In contrast an equivalent system using a phosphonated group alone to bind to NiO only had an initial coverage of ~4 nmol cm^{-2}, with the catalyst completely desorbing during use.[23] The group of Meyer have recently reported the use of Silane binding groups to link a vinyl group-containing Ru absorber (poly(Ru^{II})) on the surface of p-type NiO photoelectrodes *via* electropolymerisation in order to build a DSPEC.[115] The CO_2 reduction centre, a Re polypyridil complex (poly(Re^I)) was then bound to the poly(Ru^{II}) also by electropolymerisation. The photocathode was able to reduce CO_2 to CO under illumination and applied bias and it showed a good degree of stability, with more than 80% of the initial

photocurrents being maintained after *ca.* 10 hours of photoelectrolysis. The prolonged activity is a result of the strong Si-O bonds compared with equivalent phosphonated catalysts which showed rapid loss in activity. Transient absorption spectroscopy on the ns-µs range, was used to follow the rate of electron transfer. It was found that the rate of recombination of the catalytically active state ($NiO(h^+)$-poly(Ru^I)-poly(Re^0)) was very slow (µs-ms) suggesting that the presence of the aliphatic chains connecting the metal complexes to the NiO surface may be an important factor in achieving a long-lived charge separated state and high levels of DSPEC activity.
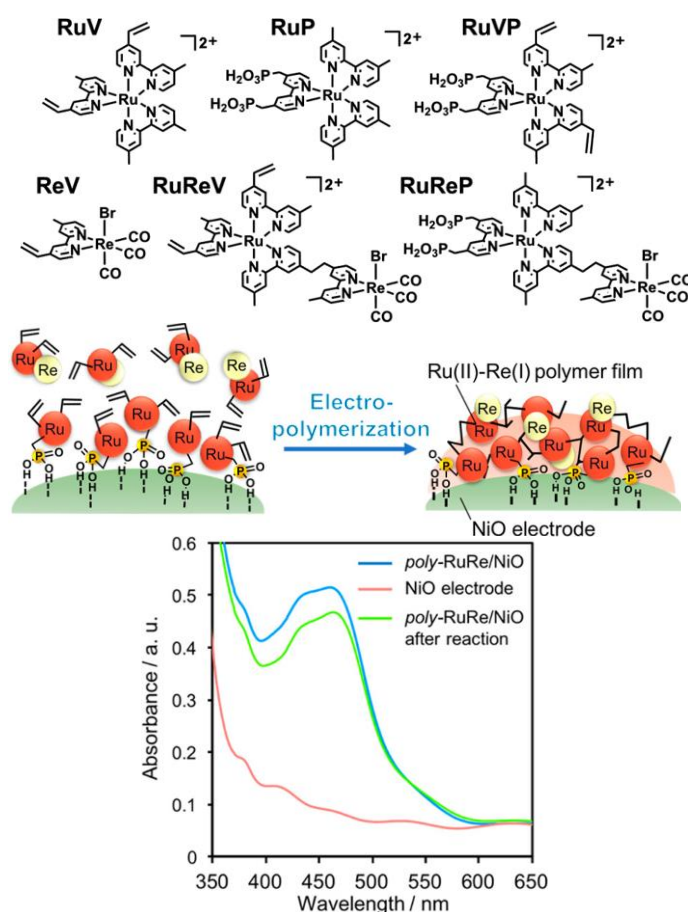
Figure 8. *Electropolymerisation of a Ru-Re dyad on NiO improved the photocathode stability compared to when relying only on the phosphonate covalent bond to the SC, and the UV-vis spectra of the film after 5 hours of bulk electrolysis showing only minimal loss of the polymeric film. Reproduced with permission from*[23]

Many of the studies outlined above contain time-resolved absorption and emission data providing evidence that using a supramolecular[116,117] DSPEC assembly for CO_2 reduction, where the chromophore is reductively quenched prior to transfer the photoelectron to a distant catalytic centre, does increase efficiency due to decreased recombination losses. The role of linking ligands on the rate of electron transfer within Ru-Re dyads for photocatalytic CO_2 reduction has also been studied in detail using time-resolved infrared spectroscopy.[116,117] With these systems, it has been shown that with alkyl ligands through bond electron transfer occurs, generating the one electron reduced Re species with the logarithm of the rate of electron transfer showing a linear relationship with the alkyl chain length. To date alkyl linkages have dominated within the DSPEC CO_2 reduction electrodes reported, however DSPEC for H_2 evolution have demonstrated that in addition to controlling the distance of charge separation it is also necessary to consider the electronic structure of the ligands[118] with approaches such as utilisation of push-pull structures proving particularly effective.[119]

The difficulty of synthesis of the complex molecular architectures is potentially a major drawback which may limit the emergence of more complex structures for use in DSPEC. Recently a simple approach was reported[109] where each component (electron donor, dye, catalyst) was added in a layer-by-layer approach on mesoporous NiO using Zr-phosphonate bridges between each component. The phosphonated dianiline donor positioned between the NiO semiconductor and the dye ([Ru((4,4′-$(PO_3H_2CH_2)_2$-2,2′-bipyridine)(2,2′-bipyridine))$_2$]$^{2+}$),[96] played a critical role leading to a *ca.* 8 times higher photocurrents (at -0.54 V_{NHE}) when the donor was present compared to photoelectrodes composed of only dye and catalyst ([Re(I)((4,4'-$PO_3H_2CH_2)_2$-2,2'-bipyridine)(CO)$_3$Cl]). While the stability of the photoelectrodes was in this example quite low, further studies by the same research group[108] showed a marked increase in stability when using a binary p-n junction with a protective coating. Here *n*-type GaN nanowires were deposited on n^+-*p*-p^+ silicon wafer, Si/*n*-GaN with

26

a sub nm thick NiO or Al_2O_3 overlayer to stabilise the phosphonate linkage to the surface, was interfaced with a range of phenylene diamine donors. Stable photocurrents of 1 mA cm^{-2} were achieved for an impressive 20 hours with HCOOH as the CO_2 reduction product. Transient absorption and emission spectroscopy of the self-assembled DSPEC photoelectrodes[108] revealed that the electrodes with the highest activity were the ones with the donor with the most positive reduction potential, confirming that a high driving force between the photoelectrode components was highly desirable.

In addition to the stability of the linkage of the supramolecular construct to the *p*-type electrode, it is also important to improve the stability of the dye itself. In a recent paper,[120] $CuInS_2$ quantum dots were deposited on NiO. The quantum dots could form a stable bond by using the COOH terminations of the cysteine ligands present. The catalyst employed was *fac*-[Re(4,4'-Bis(diethoxyphosphorylmethyl)-2,2'-bipyridine)(CO)$_3$Cl], which was deposited on the NiO/CuInS$_2$ matrix. The photoelectrode was able to reduce CO_2 to CO in a DMF solution at -0.87 V_{NHE} under illumination with a FE of 32%.

5. Future challenges for hybrid photocathodes for CO_2 reduction: The examples of photoelectrodes described in section 4 demonstrate the dual role of the hybrid structure in enabling both catalysis and charge separation. However, to move hybrid photocathodes for CO_2 reduction beyond being a solely academic pursuit step-changes in both the stability and solar energy to stored chemical fuel efficiencies are needed.

Of greatest priority is to massively improve the stability of photoelectrodes from the current state of the art (~10-20 hours) [68,108,121] to several thousand hours of use.[122] This will require advances in the design of the catalysts, dyes and also of the semiconductor/catalyst and semiconductor/dye/catalyst interface. Despite being used in some of the very earliest studies,[89]

polymerised catalysts have consistently led to the formation of layers with some of the highest stabilities, however this is often at the cost of control of catalyst orientation making it hard to design effective charge transfer interfaces.[23] Therefore recent advances making use of multifunctional coatings consisting of redox active centres with functionalities to covalently bind to the electrode surface in a controllable manner and catalytic centres with polymerisable groups are particularly exciting. [59,60] Alternatively an interesting approach being explored for immobilising water splitting and CO_2 electrocatalysts[108,114] onto supports is to use thin (sub nm) oxide layers to partially bury the catalytic centre. By embedding the binding group in a metal oxide layer large increases in stability have been reported and through careful control of the coating process it is possible to leave the catalytic site un-hindered. Great advances have been achieved using atomic layer deposition to protectively coat absorbers with thick metal oxide layers (such as TiO_2, AZO) enabling stable oxygen and hydrogen evolution[123,124] for hundreds of hours and it will be exciting to see if through a combination of these two approaches it will possible to achieve both protection of the light absorbing semiconductor and the stabilisation of a semiconductor/catalyst interface consisting of catalytic units bound in a well-defined geometry.

Transient absorption spectroscopy has shown a correlation between the photoelectrochemical activity and the lifetime of the charge separated state formed following photo absorption.[76,115,125] Therefore a continued focus on the design of the semiconductor/(dye)catalyst interface is likely to yield continued improvements in electrode efficiency by enabling both effective charge transfer away from the light absorber and through preventing back electron transfer. A major advantage of molecular electrocatalysts is that it should in principle be possible to design and synthesise catalysts to bind to the surface in a manner optimal for charge transfer. However, such design will need a greater application of spectroscopic methods that are able to identify catalyst geometry on the electrode surface.

Techniques, such as vibrational sum frequency generation (VSFG) spectroscopy do exist that are able to provide this information[126] and a series of studies have explored the orientation of Re(R-bpy)(CO)$_3$Cl derivatives bound to TiO$_2$ surfaces.[127,128] It was also essential to develop catalysts with functional groups that enable stable surface immobilisation with a well-defined geometry. Knowledge gained from the water splitting community indicates that hydroxamate anchor groups may be particularly promising as they are able to form stable, strong linkages to many of the semiconductor materials of interest and they have been shown to allow for fast electron transfer to the catalytic centre.[104]

It is also important to consider the efficiency of electron transfer to the semiconductor/catalyst interface following photon absorption. The application of a bias to the electrode to control interfacial band bending provides one route to lowering recombination and to enabling electron transport to the interface,[101,107] however it comes at an energetic cost. An alternative approach is to tune the interface energetics through the modification of the electrode with a species with a large dipole moment to induce band-bending. Interface engineering through the addition of a dipole layer has been demonstrated within the photovoltaics community[129] and in some systems for PEC water splitting.[130–133] To generate the dipole layer self-assembled monolayers of either carboxylic or phosphonic acids are often added to the semiconductor surface, but this approach is problematic due to both the low stability of the layer and due to shielding of the dipole by the electrolyte. [28,130,133] A recent development in this field has been reported by Tilley and co-workers,[133] where the introduction of a phosponic acid layer of 2 nm of thickness at the interface of p-Si and TiO$_2$ created a stable "buried junction" protecting the dipole and increasing the photovoltage by over 400 mV for a PEC electrode for hydrogen evolution. To the best of our knowledge, the use of tunable dipole layers or even the possible role of the existing used phosphonate and carboxylate anchor groups in band-edge engineering during PEC CO$_2$ reduction, has not been explored but the recent demonstration of a methodology to

29

form a stable dipole layer in an aqueous environment is an exciting opportunity for the field of CO_2 reduction.

6. Conclusions

In the absence of a catalytic centre, the slow kinetics of charge transfer across the electrode/electrolyte interface are expected to lead charge accumulation and increased recombination during PEC CO_2 reduction. The construction of hybrid semiconductor-molecular catalyst materials has been demonstrated to be an effective route to improved selectivity's and activities for carbon dioxide reduction. Here following a brief introduction to the underlying principles of photoelectrochemistry, we have introduced the rationale of the need for hybrid photoelectrodes and a survey of the main classes of these exciting materials. However, despite great progress further advances in both the solar to fuel efficiency and stability of devices is needed.

Clearly there is still much to understand about the interaction between the semiconductor and the catalyst and how this changes the nature of the interface kinetics and the mechanism of the reactions. If the community is to realise the potential tenability and control of the semiconductor/molecular catalyst interface, an improved understanding of these factors will be vital. Therefore, there is both a gap in knowledge and an exciting opportunity through which the community may learn how to make new improved photoelectrodes.

Abbreviations

$\Delta\phi_{sc}$	Potential drop across the space charge region
ε_0	Vacuum permittivity
ε_{sc}	Relative permittivity of the semiconductor material
ALD	Atomic layer deposition

AZO	Aluminium-doped zinc oxide
bpy	2,2′-Bipyridine
cat	Catalyst
cyclam	1,4,8,11-tetraazacyclotetradecane
dcbpy	4,4′-dicarboxy-2,2′-bipyridine
DMF	Dimethylformamide
DSPEC	Dye sensitised photoelectrochemical cell
DSPEC	Photoelectrosynthesis cells
DSSC	Dye-sensitised solar cell
E_C	Conduction band
E_{cat}	Onset potential of catalysis
E_F	Fermi level
E_g	Band gap
E_{red}	Redox Fermi level of the electrolyte
E_V	Valence band
FE	Faradaic efficiency
IPCE	Incident photon-to-current efficiency
MeCN	Acetonitrile
N_d	Doping density
$_nE_F^*$	Quasi electron Fermi level
NHE	Normal Hydrogen Electrode
PEC	Photoelectrochemistry
$_pE_F^*$	Quasi hole Fermi level
PS	Photosensitiser or dye
q	Elementary charge
qPyH	2,2′:6′,2″:6″,2‴-quaterpyridine
RHE	Reversible Hydrogen Electrode
SCLJ	Semiconductor liquid junction
TEOA	Triethanolamine
tpy	2,2′;6′,2″-terpyridine
V_{ph}	Photovoltage
VSFG	Vibrational sum frequency generation
W_{sc}	Space charge region
ΔG_{ET}	Gibbs free energy change for electron transfer

Conflicts of interest

There are no conflicts to declare.

Keywords

CO_2 reduction, molecular catalysts, photocathodes, photoelectrochemistry.

Notes and references

[1]   J. Barber, *Chem. Soc. Rev.* **2009**, *38*, 185–196.

[2]   L. Hammarström, *Acc. Chem. Res.* **2009**, *42*, 1859–1860.

[3]   M. Aresta, A. Dibenedetto, A. Angelini, *Chem. Rev.* **2014**, *114*, 1709–1742.

[4]   S. C. Roy, O. K. Varghese, M. Paulose, C. A. Grimes, *ACS Nano* **2010**, *4*, 1259–1278.

[5]   D. U. Nielsen, X. M. Hu, K. Daasbjerg, T. Skrydstrup, *Nat. Catal.* **2018**, *1*, 244–254.

[6]   J. L. White, M. F. Baruch, J. E. Pander, Y. Hu, I. C. Fortmeyer, J. E. Park, T. Zhang, K. Liao, J. Gu, Y. Yan, T. W. Shaw, E. Abelev, A. B. Bocarsly, *Chem. Rev.* **2015**, *115*, 12888–12935.

[7]   C. E. Creissen, M. Fontecave, *Adv. Energy Mater.* **2020**, *2002652*, 1–12.

[8]   S. Nitopi, E. Bertheussen, S. B. Scott, X. Liu, A. K. Engstfeld, S. Horch, B. Seger, I. E. L. Stephens, K. Chan, C. Hahn, J. K. Nørskov, T. F. Jaramillo, I. Chorkendorff, *Chem. Rev.* **2019**, *119*, 7610–7672.

[9]   F. Franco, C. Rettenmaier, H. S. Jeon, B. R. Cuenya, *Chem. Soc. Rev.* **2020**, *49*, 6884–6946.

[10]   T. Haas, R. Krause, R. Weber, M. Demler, G. Schmid, *Nat. Catal.* **2018**, *1*, 32–39.

[11]   J. Albero, Y. Peng, H. Garc, *ACS Catal.* **2020**, *10*, 5734−5749.

[12] H. Huang, B. Pradhan, J. Hofkens, J. A. Steele, *ACS Energy Lett.* **2020**, *5*, 1107−1123.

[13] C. Xu, J. Hong, P. Sui, M. Zhu, Y. Zhang, J.-L. Luo, *Cell Reports Phys. Sci.* **2020**, *1*, 100101.

[14] Q. Wang, J. Warnan, S. Rodríguez-Jiménez, J. J. Leung, S. Kalathil, V. Andrei, K. Domen, E. Reisner, *Nat. Energy* **2020**, *5*, 703–710.

[15] L. Zhang, Z. J. Zhao, T. Wang, J. Gong, *Chem. Soc. Rev.* **2018**, *47*, 5423–5443.

[16] X. Chang, T. Wang, P. Yang, G. Zhang, J. Gong, *Adv. Mater.* **2018**, *1804710*, 1–13.

[17] S. Xie, Q. Zhang, G. Liu, Y. Wang, *Chem. Commun.* **2016**, *52*, 35–59.

[18] V. Kumaravel, J. Bartlett, S. C. Pillai, *ACS Energy Lett.* **2020**, *5*, 486–519.

[19] P. Ding, T. Jiang, N. Han, Y. Li, *Mater. Today Nano* **2020**, *10*, DOI 10.1016/j.mtnano.2020.100077.

[20] B. Kumar, J. M. Smieja, C. P. Kubiak, *J. Phys. Chem. C* **2010**, *114*, 14220–14223.

[21] M. Schreier, J. Luo, P. Gao, T. Moehl, M. T. Mayer, M. Grätzel, *J. Am. Chem. Soc.* **2016**, *138*, 1938–1946.

[22] J. A. Esterhuizen, N. M. Orchanian, L. E. Hong, S. C. Marinescu, D. A. Popov, J. A. Skrainka, *ACS Appl. Energy Mater.* **2018**, *2*, 110–123.

[23] R. Kamata, H. Kumagai, Y. Yamazaki, G. Sahara, O. Ishitani, R. Abe, M. Higashi, T. Morikawa, K. Maeda, Y. Ueda, O. Ishitani, *ACS Appl. Mater. Interfaces* **2018**, *11*, 5632–5641.

[24] Z. Zhang, J. T. Yates, *Chem. Rev.* **2012**, *112*, 5520–5551.

[25] L. M. Peter, in *RSC Energy Environ. Ser.*, Royal Society Of Chemistry, **2016**, pp. 3–28.

[26]   A. J. Nozik, *Annu. Rev. Phys. Chem.* **1978**, *29*, 189–222.

[27]   H. Gerischer, *J. Electroanal. Chem.* **1977**, *82*, 133–143.

[28]   W. A. Smith, I. D. Sharp, N. C. Strandwitz, J. Bisquert, *Energy Environ. Sci.* **2015**, *8*, 2851–2862.

[29]   W. W. Gartner, *Phys. Rev.* **1959**, *116*, 84–87.

[30]   A. J. Bard, A. B. Bocarsly, F. R. F. Fan, E. G. Walton, M. S. Wrighton, *J. Am. Chem. Soc.* **1980**, *102*, 3671–3677.

[31]   J. Bisquert, G. Garcia-Belmonte, F. Fabregat-Santiago, *J. Solid State Electrochem.* **1999**, *3*, 337–347.

[32]   W. J. Albery, P. N. Bartlett, *J. Electrochem. Soc.* **1984**, *131*, 315–325.

[33]   B. P. (B. P. Sullivan, K. Krist, H. E. Guard, *Electrochemical and Electrocatalytic Reactions of Carbon Dioxide*, Elsevier, **1993**.

[34]   B. Kumar, M. Llorente, J. Froehlich, T. Dang, A. Sathrum, C. P. Kubiak, in *Annu. Rev. Phys. Chem. Vol 63* (Ed.: M.A.M.T.J. Johnson), **2012**, pp. 541-+.

[35]   L. Junfu, C. Y. Baozhu, *J. Electroanal. Chem.* **1992**, *324*, 191–200.

[36]   H. Yoneyama, K. Sugimura, S. Kuwabata, *J. Electroanal. Chem.* **1988**, *249*, 143–153.

[37]   B. Aurian-Blajeni, M. Halmann, J. Manassen, *Sol. Energy Mater.* **1983**, *8*, 425–440.

[38]   M. Halmann, *Nature* **1978**, *275*, 115–116.

[39]   J. Schneider, H. Jia, J. T. Muckerman, E. Fujita, *Chem. Soc. Rev.* **2012**, *41*, 2036–2051.

[40]   I. Taniguchi, B. Aurian-Blajeni, J. O. Bockris, *Electrochim. Acta* **1984**, *29*, 923–932.

[41]   Y. J. Jang, J. W. Jang, J. Lee, J. H. Kim, H. Kumagai, J. Lee, T. Minegishi, J. Kubota,

K. Domen, J. S. Lee, *Energy Environ. Sci.* **2015**, *8*, 3597–3604.

[42]   J. O. Bockris, J. C. Wass, *Mater. Chem. Phys.* **1989**, *22*, 249–280.

[43]   J. S. Duchene, G. Tagliabue, A. J. Welch, W. H. Cheng, H. A. Atwater, *Nano Lett.* **2018**, *18*, 2545–2550.

[44]   K. A. Grice, *Coord. Chem. Rev.* **2017**, *336*, 78–95.

[45]   Y. Wang, D. He, H. Chen, D. Wang, *J. Photochem. Photobiol. C Photochem. Rev.* **2019**, 1–33.

[46]   M. Stanbury, J.-D. Compain, S. Chardon-Noblat, *Coord. Chem. Rev.* **2018**, *361*, 120–137.

[47]   R. Francke, B. Schille, M. Roemelt, *Chem. Rev.* **2018**, *118*, 4631–4701.

[48]   K. Elouarzaki, V. Kannan, V. Jose, H. S. Sabharwal, J. M. Lee, *Adv. Energy Mater.* **2019**, *9*, 1–33.

[49]   S. Ren, D. Joulié, D. Salvatore, K. Torbensen, M. Wang, M. Robert, C. P. Berlinguette, *Science (80-.).* **2019**, *365*, 367–369.

[50]   C. Costentin, M. Robert, J.-M. M. Savéant, A. Tatin, *Proc. Natl. Acad. Sci. U. S. A.* **2015**, *112*, 6882–6886.

[51]   S. Zhang, Q. Fan, R. Xia, T. J. Meyer, *Acc. Chem. Res.* **2019**, DOI 10.1021/acs.accounts.9b00496.

[52]   L. Sun, V. Reddu, A. C. Fisher, X. Wang, *Energy Environ. Sci.* **2020**, *13*, 374–403.

[53]   D. Nam, P. De Luna, A. Rosas-hernández, A. Thevenon, F. Li, T. Agapie, J. C. Peters, O. Shekhah, M. Eddaoudi, E. H. Sargent, *Nat. Mater.* **2020**, *19*, 266–276.

[54]   A. Wagner, C. D. Sahm, E. Reisner, *Nat. Catal.* **n.d.**, DOI 10.1038/s41929-020-00512-

x.

[55] K. E. Dalle, J. Warnan, J. J. Leung, B. Reuillard, I. S. Karmel, E. Reisner, *Chem. Rev.* **2019**, *119*, 2752–2875.

[56] K. Maeda, *Adv. Mater.* **2019**, *1808205*, DOI 10.1002/adma.201808205.

[57] E. Boutin, L. Merakeb, B. Ma, B. Boudy, M. Wang, J. Bonin, E. Anxolabéhère-Mallart, M. Robert, *Chem. Soc. Rev.* **2020**, *49*, 5772–5809.

[58] T. Arai, S. Sato, K. Uemura, T. Morikawa, T. Kajino, T. Motohiro, *Chem. Commun.* **2010**, *46*, 6944–6946.

[59] S. Sato, T. Arai, T. Morikawa, K. Uemura, T. M. Suzuki, H. Tanaka, T. Kajino, *J. Am. Chem. Soc.* **2011**, *133*, 15240–15243.

[60] T. Arai, S. Tajima, S. Sato, K. Uemura, T. Morikawa, T. Kajino, *Chem. Commun.* **2011**, *47*, 12664–12666.

[61] A. Paracchino, N. Mathews, T. Hisatomi, M. Stefik, S. D. Tilley, M. Grätzel, *Energy Environ. Sci.* **2012**, *5*, 8673–8681.

[62] S. Sato, T. Morikawa, S. Saeki, T. Kajino, T. Motohiro, *Angew. Chemie-International Ed.* **2010**, *49*, 5101–5105.

[63] M. Beley, J. P. Collin, R. Ruppert, J. P. Sauvage, *J. Am. Chem. Soc.* **1986**, *108*, 7461–7467.

[64] G. Neri, I. M. Aldous, J. J. Walsh, L. J. Hardwick, A. J. Cowan, *Chem. Sci.* **2016**, *7*, 1521–1526.

[65] M. Bourrez, F. Molton, S. Chardon-Noblat, A. Deronzier, *Angew. Chem. Int. Ed. Engl.* **2011**, *50*, 9903–9906.

[66] J. J. Walsh, G. Neri, C. L. Smith, A. J. Cowan, *Chem. Commun.* **2014**, *50*, 12698–12701.

[67] J. Hawecker, J.-M. Lehn, R. Ziessel, *J. Chem. Soc. Chem. Commun.* **1984**, *0*, 328–330.

[68] J. J. Leung, J. Warnan, K. H. Ly, N. Heidary, D. H. Nam, M. F. Kuehnel, E. Reisner, V. Kumaravel, J. Bartlett, S. C. Pillai, J. J. Leung, J. Warnan, K. H. Ly, N. Heidary, D. H. Nam, M. F. Kuehnel, E. Reisner, *Nat. Catal.* **2019**, *2*, 354–365.

[69] K. Yamanaka, S. Sato, M. Iwaki, T. Kajino, T. Morikawa, *J. Phys. Chem. C* **2011**, *115*, 18348–18353.

[70] M. G. Bradley, T. Tysak, D. J. Graves, N. A. Vlachopoulos, N. A. Vlachopoulosc, *J. Chem. Soc.* **1983**, *Journal of*, 349–350.

[71] M. G. Bradley, T. Tysak, *J. Electroanal. Chem.* **1982**, *135*, 153–157.

[72] D. He, T. Jin, W. Li, S. Pantovich, D. Wang, G. Li, *Chem. - A Eur. J.* **2016**, *22*, 13064–13067.

[73] E. Torralba-Penalver, Y. Luo, J. D. Compain, S. Chardon-Noblat, B. Fabre, *ACS Catal.* **2015**, *5*, 6138–6147.

[74] A. J. Cowan, J. R. Durrant, *Chem. Soc. Rev.* **2013**, *42*, 2281–2293.

[75] T. M. Suzuki, H. Tanaka, T. Morikawa, M. Iwaki, S. Sato, S. Saeki, M. Inoue, T. Kajino, T. Motohiro, *Chem. Commun.* **2011**, *47*, 8673.

[76] G. Neri, J. J. Walsh, C. Wilson, A. Reynal, J. Y. C. Lim, X. Li, A. J. P. White, N. J. Long, J. R. Durrant, A. J. Cowan, *Phys. Chem. Chem. Phys.* **2015**, *17*, 1562–1566.

[77] K. Sekizawa, S. Sato, T. Arai, T. Morikawa, *ACS Catal.* **2018**, *8*, 1405–1416.

[78] M. Beley, J.-P. Collin, R. Ruppert, J.-P. Sauvage, *J. Chem. Soc. Chem. Commun.* **1984**, *2*, 1315–1316.

[79] J.-P. Petit, P. Chartier, M. Beley, J.-P. Deville, *J. Electroanal. Chem.* **1989**, *269*, 267–281.

[80] M. Beley, J. P. Collin, J. P. Sauvage, J. P. Petit, P. Chartier, *J. Electroanal. Chem.* **1986**, *206*, 333–339.

[81] K. Alenezi, S. K. Ibrahim, P. Li, C. J. Pickett, *Chem. - A Eur. J.* **2013**, *19*, 13522–13527.

[82] E. E. Barton, D. M. Rampulla, A. B. Bocarsly, *J. Am. Chem. Soc.* **2008**, *130*, 6342-+.

[83] M. Schreier, P. Gao, M. T. Mayer, J. Luo, T. Moehl, M. K. Nazeeruddin, S. D. Tilley, M. Grätzel, *Energy Environ. Sci.* **2015**, *8*, 855–861.

[84] C. D. Windle, E. Pastor, A. Reynal, A. C. Whitwood, Y. Vaynzof, J. R. Durrant, R. N. Perutz, E. Reisner, *Chem. - A Eur. J.* **2015**, *21*, 3746–3754.

[85] B. Zhao, H. Lei, N. Wang, G. Xu, W. Zhang, R. Cao, *Chem. – A Eur. J.* **2019**, 1–7.

[86] T. Jin, D. He, W. Li, C. J. Stanton, S. A. Pantovich, G. F. Majetich, H. F. Schaefer, J. Agarwal, D. Wang, G. Li, *Chem. Commun.* **2016**, *52*, 14258–14261.

[87] H. Tian, *ChemSusChem* **2015**, *8*, 3746–3759.

[88] E. Torralba-Penalver, Y. Luo, J. D. Compain, S. Chardon-Noblat, B. Fabre, *ACS Catal.* **2015**, *5*, 6138–6147.

[89] C. R. Cabrera, H. D. Abruña, *J. Electroanal. Chem.* **1986**, *209*, 101–107.

[90] R. Aydin, F. Köleli, *Synth. Met.* **2004**, *144*, 75–80.

[91] F. Koleli, T. Ropke, C. Hamann, *Synth. Met.* **2004**, *140*, 65–68.

[92] J. J. Leung, J. A. Vigil, J. Warnan, E. Edwardes Moore, E. Reisner, *Angew. Chemie - Int. Ed.* **2019**, *58*, 7697–7701.

[93]   M. F. Kuehnel, C. D. Sahm, G. Neri, J. R. Lee, K. L. Orchard, A. J. Cowan, E. Reisner, *Chem. Sci.* **2018**, *9*, 2501–2509.

[94]   M. F. Kuehnel, K. L. Orchard, K. E. Dalle, E. Reisner, *J. Am. Chem. Soc.* **2017**, *139*, 7217–7223.

[95]   J. Huang, K. L. Mulfort, P. Du, L. X. Chen, *J. Am. Chem. Soc.* **2012**, *134*, 16472–16475.

[96]   L. Zhang, J. M. Cole, *ACS Appl. Mater. Interfaces* **2015**, *7*, 3427–3455.

[97]   K. L. Materna, R. H. Crabtree, G. W. Brudvig, *Chem. Soc. Rev.* **2017**, *46*, 6099–6110.

[98]   R. Ernstorfer, L. Gundlach, S. Felber, W. Storck, R. Eichberger, F. Willig, *J. Phys. Chem. B* **2006**, *110*, 25383–25391.

[99]   A. V. Akimov, R. Asahi, R. Jinnouchi, O. V. Prezhdo, *J. Am. Chem. Soc.* **2015**, *137*, 11517–11525.

[100]   G. Neri, M. Forster, J. J. Walsh, C. M. Robertson, T. J. Whittles, P. Farràs, A. J. Cowan, *Chem. Commun.* **2016**, *52*, 14200–14203.

[101]   C. Bozal-Ginesta, C. A. Mesa, A. Eisenschmidt, L. Francas, R. B. Shankar, D. Anton-Garcia, J. Warnan, J. Willkomm, A. Reynal, E. Reisner, J. R. Durrant, *Chem. Sci.* **2020**, DOI 10.1039/d0sc04344c.

[102]   P. B. Pati, R. Wang, E. Boutin, S. Diring, S. Jobic, N. Barreau, F. Odobel, M. Robert, *Nat. Commun.* **2020**, *11*, 1–9.

[103]   A. Paracchino, V. Laporte, K. Sivula, M. Graetzel, E. Thimsen, *Nat. Mater.* **2011**, *10*, 456–461.

[104]   W. R. McNamara, R. L. Milot, H. E. Song, R. C. Snoeberger, V. S. Batista, C. A. Schmuttenmaer, G. W. Brudvig, R. H. Crabtree, *Energy Environ. Sci.* **2010**, *3*, 917–923.

[105] L. Gong, H. Yin, C. Nie, X. Sun, X. Wang, M. Wang, *ACS Appl. Mater. Interfaces* **2019**, *11*, 34010−34019.

[106] M. L. Clark, P. L. Cheung, M. Lessio, E. A. Carter, C. P. Kubiak, *ACS Catal.* **2018**, *8*, 2021–2029.

[107] X. Xiong, M. Forster, J. D. Major, Y. Xu, A. J. Cowan, *J. Phys. Chem. C* **2017**, *121*, 22073–22080.

[108] B. Shan, S. Vanka, T.-T. Li, L. Troian-Gautier, M. K. Brennaman, Z. Mi, T. J. Meyer, *Nat. Energy* **2019**, *4*, 290–299.

[109] D. Wang, Y. Wang, M. D. Brady, M. V. Sheridan, B. D. Sherman, B. H. Farnum, Y. Liu, S. L. Marquard, G. J. Meyer, C. J. Dares, T. J. Meyer, *Chem. Sci.* **2019**, *10*, 4436–4444.

[110] Y. Kou, S. Nakatani, G. Sunagawa, Y. Tachikawa, D. Masui, T. Shimada, S. Takagi, D. A. Tryk, Y. Nabetani, H. Tachibana, H. Inoue, *J. Catal.* **2014**, *310*, 57–66.

[111] G. Sahara, R. Abe, M. Higashi, T. Morikawa, K. Maeda, Y. Ueda, O. Ishitani, *Chem. Commun.* **2015**, *51*, 10722–10725.

[112] G. Sahara, H. Kumagai, K. Maeda, N. Kaeffer, V. Artero, M. Higashi, R. Abe, O. Ishitani, *J. Am. Chem. Soc.* **2016**, *138*, 14152–14158.

[113] H. Kumagai, G. Sahara, K. Maeda, M. Higashi, R. Abe, O. Ishitani, *Chem. Sci.* **2017**, *8*, 4242–4249.

[114] M. K. Brennaman, R. J. Dillon, L. Alibabaei, M. K. Gish, C. J. Dares, D. L. Ashford, R. L. House, G. J. Meyer, J. M. Papanikolas, T. J. Meyer, *J. Am. Chem. Soc.* **2016**, *138*, 13085–13102.

[115] T.-T. Li, B. Shan, T. J. Meyer, *ACS Energy Lett.* **2019**, *4*, 629–636.

[116] Y. Yamazaki, K. Ohkubo, D. Saito, T. Yatsu, Y. Tamaki, S. Tanaka, K. Koike, K. Onda, O. Ishitani, *Inorg. Chem.* **2019**, *58*, 11480–11492.

[117] K. Koike, D. C. Grills, Y. Tamaki, E. Fujita, K. Okubo, Y. Yamazaki, M. Saigo, T. Mukuta, K. Onda, O. Ishitani, *Chem. Sci.* **2018**, *9*, 2961–2974.

[118] N. Põldme, L. O'Reilly, I. Fletcher, J. Portoles, I. V. Sazanovich, M. Towrie, C. Long, J. G. Vos, M. T. Pryce, E. A. Gibson, *Chem. Sci.* **2019**, *10*, 99–112.

[119] N. Kaeffer, J. Massin, C. Lebrun, O. Renault, M. Chavarot-Kerlidou, V. Artero, *J. Am. Chem. Soc.* **2016**, *138*, 12308–12311.

[120] J. Huang, B. Xu, L. Tian, P. B. Pati, A. S. Etman, J. Sun, L. Hammarström, H. Tian, *Chem. Commun.* **2019**, 7918–7921.

[121] H. Zhang, Y. Chen, H. Wang, H. Wang, W. Ma, X. Zong, C. Li, *Adv. Energy Mater.* **2020**, *2002105*, 1–9.

[122] B. A. Pinaud, J. D. Benck, L. C. Seitz, A. J. Forman, Z. Chen, T. G. Deutsch, B. D. James, K. N. Baum, G. N. Baum, S. Ardo, H. Wang, E. Miller, T. F. Jaramillo, *Energy Environ. Sci.* **2013**, *6*, 1983–2002.

[123] Z. Yin, R. Fan, G. Huang, M. Shen, *Chem. Commun.* **2018**, *54*, 543–546.

[124] S. Hu, M. R. Shaner, J. A. Beardslee, M. Lichterman, B. S. Brunschwig, N. S. Lewis, *Science (80-.).* **2014**, *344*, 1005–1009.

[125] A. Reynal, J. Willkomm, N. M. Muresan, F. Lakadamyali, M. Planells, E. Reisner, J. R. Durrant, *Chem. Commun.* **2014**, *50*, 12768–12771.

[126] G. Neri, J. J. Walsh, G. Teobaldi, P. M. Donaldson, A. J. Cowan, *Nat. Catal.* **2018**, *1*,

952–959.

[127] C. L. Anfuso, D. Xiao, A. M. Ricks, C. F. A. Negre, V. S. Batista, T. Lian, *J. Phys. Chem. C* **2012**, *116*, 24107–24114.

[128] C. L. Anfuso, R. C. Snoeberger, A. M. Ricks, W. Liu, D. Xiao, V. S. Batista, T. Lian, *J. Am. Chem. Soc.* **2011**, *133*, 6922–6925.

[129] H. Bedis, *J. Surf. Eng. Mater. Adv. Technol.* **2011**, *01*, 42–50.

[130] J. M. Gurrentz, M. J. Rose, *J. Am. Chem. Soc.* **2020**, *142*, 5657–5667.

[131] S. S. Kocha, *J. Electrochem. Soc.* **2006**, *142*, 2625.

[132] B. A. Macleod, K. X. Steirer, J. L. Young, U. Koldemir, A. Sellinger, J. A. Turner, T. G. Deutsch, D. C. Olson, *ACS Appl. Mater. Interfaces* **2015**, *7*, 11346–11350.

[133] R. Wick-Joliat, T. Musso, R. R. Prabhakar, J. Löckinger, S. Siol, W. Cui, L. Sévery, T. Moehl, J. Suh, J. Hutter, M. Iannuzzi, S. D. Tilley, *Energy Environ. Sci.* **2019**, 9–12.

Table of contents: Hybrid photocathodes offer a way to achieve selective and efficient CO_2 photoelectrochemical reduction. Here we review how the design of the semiconductor/molecular catalyst interface can control charge separation, catalysis and stability.